THE JOURNAL OF PHYSICAL CHEMISTRY C

ARTICLE

pubs.acs.org/JPCC

Graphene-Based Flexible Supercapacitors: Pulse-Electropolymerization of Polypyrrole on Free-Standing Graphene Films

Aaron Davies, Philippe Audette, Blake Farrow, Fathy Hassan, Zhongwei Chen, Ja-Yeon Choi, and Aiping Yu*

Department of Chemical Engineering, Waterloo Institute for Nanotechnology, Waterloo Institute for Sustainable Energy, University of Waterloo, 200 University Avenue West, Waterloo, Ontario, Canada N2L 3G1

Supporting Information

ABSTRACT: A simple method has been implemented to create flexible, uniform graphene−polypyrrole composite films using a pulsed electropolymerization technique for supercapacitor electrodes. Applying the pseudocapacitive contribution of conformal redox-active polypyrrole to graphene supercapacitor electrodes results in high performance while still maintaining the inherent flexibility of graphene films. Specific capacitances as high as 237 F/g were obtained for a moderate total deposition time of only 120 s, which is approximately four times higher than the blank scaffold, graphene films. This flexible supercapacitor film exhibited very high energy and power densities with values of ∼33 Wh/kg and ∼1184 W/kg, respectively, at a scan rate of 0.01 V/s. This increase was attributed to the favorable nucleation of new polymer chains at defects on the graphene surface, which become less favorable as defect sites are occupied by existing polymer nanoparticles.

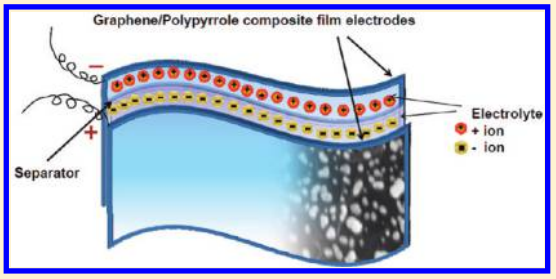

INTRODUCTION

There has recently been a growing demand for energy storage systems with high power for use in such diverse applications as hybrid electric vehicles, personal electronics, and industrial power backup.[1−6] Recent attention has focused on supercapacitors (also known as ultracapacitors or electrochemical capacitors) to address these demands.[2,6−14] Supercapacitors are a promising new energy storage system on account of the high charge−discharge rates, simple mechanism, long cycle-life, and high power density that they possess.[5,6,13−17] Focus has presently turned to the creation of flexible supercapacitors for use in various personal soft portable electronics such as cell phones and mp3 players, where flexibility is becoming an increasingly desirable quality.[18,19] Figure 1 shows a schematic representation of a flexible supercapacitor made from graphene/polypyrrole.

Supercapacitors gain their capacitive properties from two separate mechanisms; electric double-layer capacitance (EDLC) and pseudocapacitance.[5,6,9,13,15−17] EDLC is a result of the accumulation of electrostatically charged layers at the interface between the electrode and electrolyte and is therefore greatly influenced by the surface area of the electrode material.[1,6,8−10,13,15,20] To maximize EDLC, various forms of high surface area carbon have been investigated such as carbon nanotubes, activated carbon black, and graphene.[1,6,8,12,15,17,21−25] As a prominent material, graphene (G) sheets are 2D, single-atom thick layers of sp^2-bonded carbon.[26−29] These are of particular interest because it has been recently shown that optically transparent, flexible G films can be created while preserving G's good electrochemical properties.[15,19,28−35]

Pseudocapacitance is a result of reversible, fast faradic reactions occurring between an electroactive electrode material and the electrolyte.[1,6,9,10,13,15,17,20] Some pseudocapacitive materials that have been widely studied are metal oxides and electrically conducting polymers (ECPs).[1,2,4,5,8,9,13,15,17,20,21,36,37] ECPs, such as polyaniline and polypyrrole (PPy), have received much attention because of their fast electrochemical switching, low cost, and high specific capacitance values.[2,11,38−41] PPy is particularly appropriate for this application because of the water solubility of the pyrrole monomer as well as the much lower carcinogenic risks associated with its degradation products compared with polyaniline.[3,39,41]

A variety of electrode synthesis methods have been employed to create conductive polymer−carbon nanostructure heterostructures, including one-pot copolymerization, and electrodeposition on prefabricated CNT membranes. It is anticipated that the new heterostructure can bring the EDLC and pseudocapacitive behavior together, leading to a significantly enhanced performance and stability.[6,8,23,36] However, copolymerization with graphene or CNT suspensions suffers from polymeric aggregation and high electrode resistances because of poor interconnection between conducting structures, whereas post-fabrication electrodeposition often blocks electrolyte channels at the outer surface and does not form a conformal coating of polymer.[39,41,42] Much attention has been given to the pulse

Received: June 14, 2011
Revised: July 19, 2011
Published: August 04, 2011

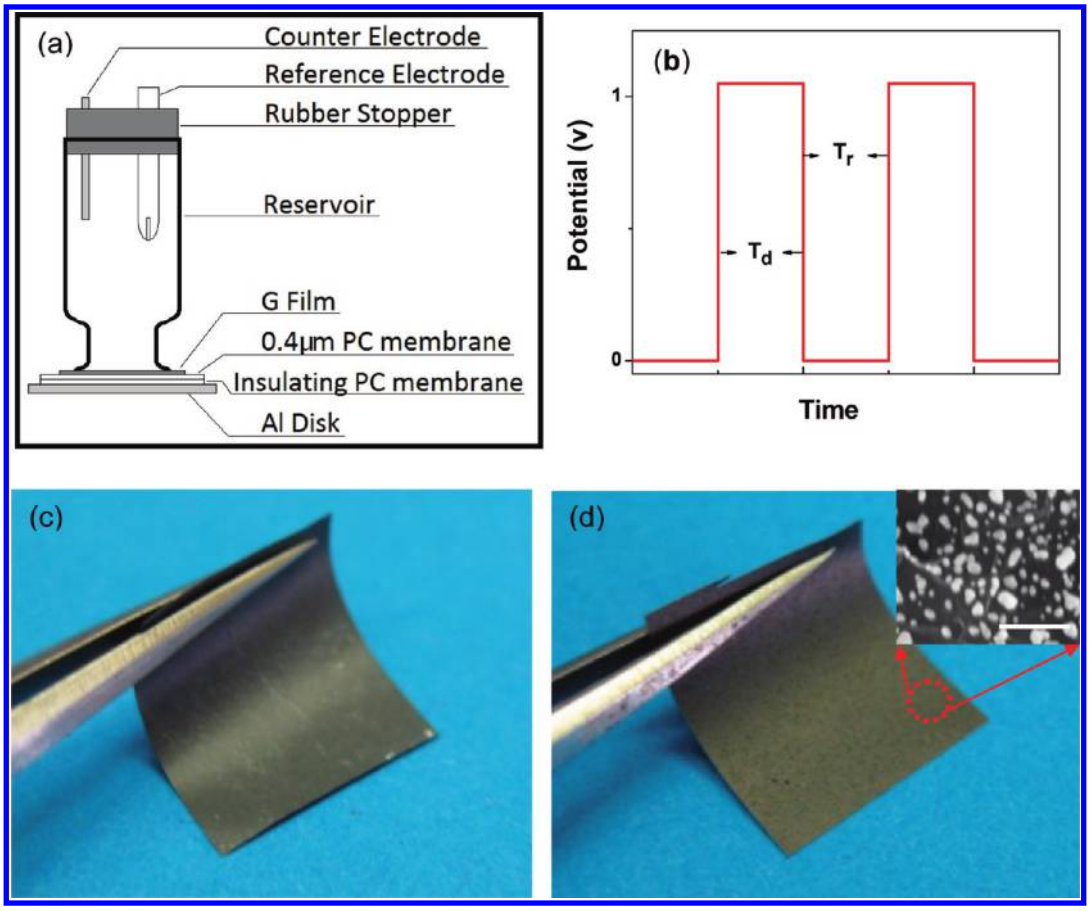

Figure 1. (a) Diagram of the apparatus used to deposit PPY on GNPs and electrochemical testing, where the clamp and rubber O-ring are not shown. (b) Electrodeposition potential waveform used in deposition experiments, with deposition pulse length T_d and rest pulse length T_r. Photographs showing the flexibility of the (c) pure GNPs and (d) G/PPy 120s films. The inset is the SEM image at the observation area; the white bar is 100 nm.

electrodeposition techniques owing to their promising results shown recently by several groups.[2,41,42] In a recent study, pulsed electrodeposition has been employed using well-separated short potential pulses, which allows pyrrole monomers to diffuse into the carbon EDLC material pore space between polymerization pulses, and demonstrated a significant improvement in the uniformity of PPy coatings on CNTs.[42] A schematic illustration showing how rest periods allow for Py molecules to diffuse into the pore space of the G between deposition pulses is shown in Figure 2. This leads to a more uniform coating and less blocked pores than obtained with a continuous deposition method. Some groups have also proposed that during rest periods polypyrrole chains stabilize, making nucleation of new chains more favorable during subsequent polymerization pulses rather than enlarging previous chains.[2,41] Short deposition pulses have also been shown to produce fewer defects in the structure of the resulting polypyrrole chains. Figure 1 shows a schematic of the pulsed electrodeposition process.

In our previous work, we have demonstrated the high efficiency of ultrathin flexible graphene films for supercapacitors.[19] In this study, graphene/polypyrrole composites were created using a modified pulsed electrodeposition technique with differing total deposition times in an effort to optimize the electrodeposition time of Py for synergistic capacitive ability. The primary objective of this study is to prepare optimized homogeneous graphene/polypyrrole composite films that give reasonably high performance for flexible supercapacitors applications.

EXPERIMENTAL SECTION

Graphite and pyrrole were purchased from Alfa and Aldrich, respectively. Reduced graphene oxide was prepared by using a modified Hummers method, which yielded individual and few-layer graphene flakes with diameters ranging from 0.1 to 1 μm.[43] Graphene films were prepared on an insulating polycarbonate membrane support. To prepare these samples, we sonicated as-prepared graphene with a concentration of 0.05 mg/mL for 1 h. This dispersion was vacuum-filtered through a polycarbonate (PC) membrane (25 mm diameter, 0.4 μm pores) to create a uniform graphene film.

The resulting graphene film on PC support membrane remained flexible and robust to washings. Typical thickness of the graphene film is ~20 μm after removal from PC membrane, which was measured by a caliper. Without removal from the PC membrane, the film was placed on a supporting aluminum disk of the apparatus shown in Figure 1a. A rubber gasket and glass electrolyte reservoir were clamped to the film over a representative and uniform region. A 1 M KCl and 50 mM pyrrole (Py) monomer solution was used to fill the reservoir, and a rubber stopper was affixed to the top of the reservoir. A three-electrode setup consisting of a Pt counter and SCE reference electrode was

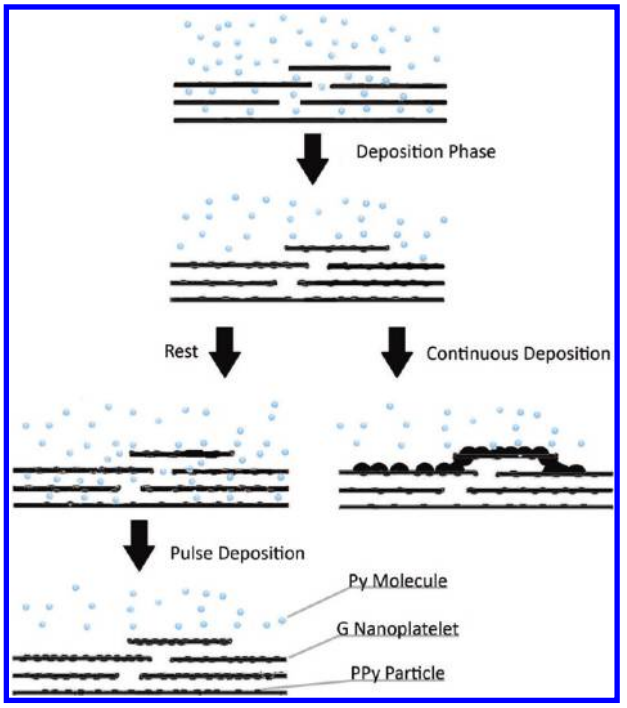

Figure 2. Schematic diagram illustrating how rest periods allow for Py molecules to diffuse into the pore space of the G between deposition pulses. This leads to a more uniform coating and fewer blocked pores than obtained with a continuous deposition method.

placed in solution through the rubber stopper. The graphene film was then wired as the working electrode.

A CHI 760D electrochemical workstation (CH Instruments, USA) was used to pulse the potential from 0 to 1.05 V for 0.1 s each until a predefined total deposition time was reached to deposit PPy uniformly onto the G. To determine the optimal PPy electrodeposition time, electrodes and films were prepared with several total electrodeposition times ranging from 60 to 360 s with 60 s intervals and are denoted G/PPy 60, G/PPy 120, G/PPy 180, G/PPy 240, G/PPy 300, and G/PPy 360, respectively, with the pure G electrode being denoted simply G. The results were focused on the G, G/PPy 60, G/PPy 120, and G/PPy 360 samples to demonstrate the concept and performances.

Electrochemical characterization was carried out using the same apparatus as above and followed by draining the deposition solution from the reservoir and rinsing the resulting composite film with deionized water. After drying at 50 °C under vacuum, the G/PPy membrane with a diameter of 25 mm was ready for use as an electrode without any further treatment. Cyclic voltametry (CV), charge discharge (CD), and electrochemical impedance spectroscopy (EIS) techniques were all carried out following a 25-cycle CV activation between −0.4 and 0.6 V versus SCE at a scan rate of 0.1 V/s in 1 M KCl electrolyte. CV was carried out between −0.4 and 0.6 V versus SCE at scan rates between 0.01 and 0.2 V/s. CD was carried out between −0.4 and 0.6 V versus SCE at current densities between 1 and 4 A/g. EIS was carried out between 1 MHz and 10 mHz under an open circuit potential (OCP) with AC signal amplitudes between 10 and 100 mV. The capacitance of the supercapacitor was calculated on the mass of the graphene films because the mass of the deposited polypyrrole was negligible by so short deposition time.

TGA was conducted on a Q500 thermogravimetric analyzer (TA Instruments, USA) in nitrogen between 50 and 800 at 10 °C/min. TGA analysis of samples involved drying at 60 °C for 72 h prior to testing. SEM images were obtained using an LEO 1550 FESEM (LEO Electron Microscopy, USA).

RESULTS AND DISCUSSION

The waveform of the shape shown in Figure 1b was applied to the GNP film in an electropolymerization solution containing 1 M KCl electrolyte and 50 mM pyrrole. The "on" potential was held at 1.05 V versus SCE for electropolymerization, and lowered to OCP during the "off" resting cycles. These waveforms were repeated until a total deposition time T_d had been reached. Figure 1c,d shows a graphene film supported on a PC membrane with a diameter of 25 mm before and after 120 s of electrodeposition of PPy. Both films are homogeneous and show good flexibility, which indicates that deposition pulses do not inhibit the flexibility of pure G. This also suggests that the feasible construction of flexible supercapacitors was able to take advantage of both EDLC and pseudocapacitance, which provides a good way to meet the increasing demands for high-energy density supercapacitors.[6,18,44]

Figure 2 illustrates the whole pulse electropolymerization process compared with the continuous electropolymerization under the waveform shown in Figure 1b. During the deposition pulse, the pyrrole monomers in the immediate vicinity of the graphene films are electropolymerized and precipitated as polypyrrole nanoparticles on the graphene surface. During continuous deposition, all pyrrole monomers suspended in the porous structure of the graphene film are consumed, leading to significantly reduced electropolymerization of monomer within the graphene. All remaining deposition current instead is consumed by electropolymerization at the film surface, where pyrrole monomer concentration is continually restored by diffusion from the bulk solution. This appearance of larger sized polymer nanoparticles is further enhanced by the likelihood for electropolymerization to continue on any given polymer chain rather than nucleate the growth of a new chain. This results in very rare nucleation of new chains on the graphene surface, which tends to enlarge present polymer particles rather than increase particle density and surface coverage. The combined effect results in large and continuous polypyrrole particles on the graphene surface (shown in continuous electropolymerization) but with very little penetration into the porous network of graphene sheets. This also reduces the surface area of the composite electrode capable of performing the fast faradaic redox reactions, which provide the additional contribution of pseudocapacitance to the device. As reported elsewhere,[42] increasing the resting time T_r between short deposition pulses allows pyrrole monomers to diffuse from the bulk solution into the intercalating spaces between graphene sheets and to be electropolymerized during the following deposition pulse. The addition of these resting periods results in uniform deposition of small polypyrrole nanoparticles throughout the porous graphene film, as shown in Figure 3, and maximizes the exposed polypyrrole surface area on the graphene sheets. The resting time further serves to allow relaxation of polymer chains grown during a previous deposition pulse. This relaxation allows polymer nanoparticles to be grown entirely in one pulse and then to relax to a lower energy state during the rest time with no further growth during subsequent pulses.[42,45] This result is likely to improve further the PPy coverage

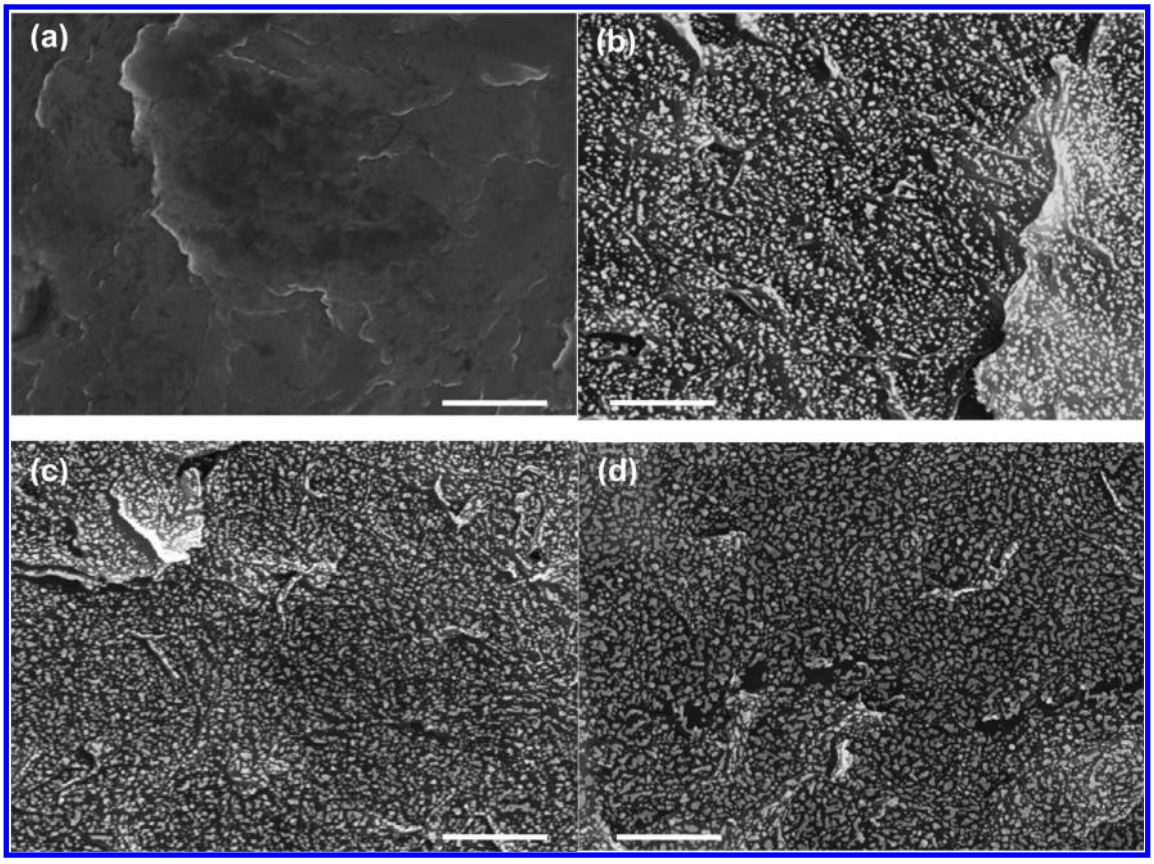

Figure 3. SEM images of (a) pure G and G/PPy after a (b) 60, (c) 120, (d) 360 s electrodeposition. The white particles are the PPy, and the white bar is 1 μm.

on the graphene electrode and increase the pseudocapacitive contribution to the specific capacitance of the composite films.

To quantify the effect of differing electrodeposition parameters on the PPy nanoparticle density and size, we used SEM, shown in Figure 3, to characterize the G/PPy composite film surfaces under various electrodeposition times. It can be seen that the films are uniform with a PPy particle number density increasing with electrodeposition time. SEM was also used for an empirical comparison of the PPy average particle size and particle area density on a nanoparticle/μm^2 basis, where images with varying total deposition time were analyzed.

The results presented in Figure 4a show a linear increase in average particle size with electrodeposition time. Previous claims suggest that pulsed depositions lead to small, stable nanoparticles, all of which are nucleated in an initial pulse.[2,41] These particle densities shown in Figure 4b appear to substantiate this growth mechanism. As shown, the particle density is increasing with longer electrodeposition times (and therefore greater number of pulses), which suggests that new particles tend to form during each deposition pulse. Combined with average particle size in Figure 4a, this suggests that many particles are able to relax during a rest pulse, allowing the preferred nucleation of new particles; however, some particles do not relax and continue growing during subsequent electrodeposition pulses. It should be noted, however, that given random self-nucleation during a new electrodeposition pulse and continually increasing particle density, it becomes increasingly likely that a new polymer strand will nucleate on a pre-existing particle, thereby resulting in the observed particle size increase. Continuous electrodeposition of polymer would likely produce a relatively constant density independent of deposition time along with an increasing particle size with increasing deposition time because added monomers tend to polymerize on pre-existing polymer chains rather than self-nucleate.[46]

It is notable that the PPy particle density does not increase linearly with deposition time. The density increases rapidly until total electrodeposition time of 120 s is reached, followed by a leveling off as the nucleation rate of new particles decreases. This represents the point at which the tendency for a new polymer chain to nucleate during a deposition pulse becomes less favorable than enlarging an existing PPy particle. The mechanism behind this change in nucleation tendency is likely due to the presence of oxidized defects in the graphene surface, which have been shown to be preferred nucleation sites for crystallite and polymer nucleation.[46,47] Once nucleation has occurred on most of these oxidative defects, the energy expenditure for self-nucleation of a new polymer strand increases, making enlargement of an existing strand more energetically favorable.

To gain a more complete analysis of the growth trends at different total deposition times, we calculated the particle size distributions at total deposition times of 60, 120, and 360 s, as shown in Figure 4c. At low deposition times, the vast majority of PPy nanoparticles are under 10 nm in diameter, suggesting that most nanoparticles have not grown for more than a single deposition cycle, and nucleation of new nanoparticles is more favorable than enlargement of existing nanoparticles. This peak is notably diminished after 120 s of deposition, with a new broad secondary peak appearing for particles with diameters between

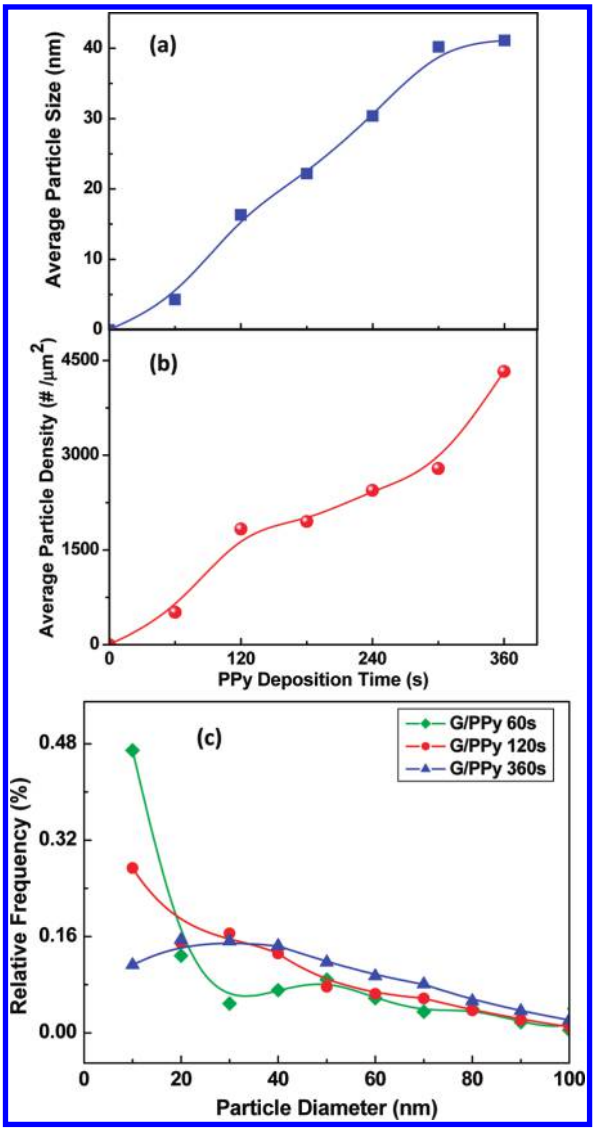

Figure 4. (a) Average PPy particle diameter and (b) average PPy particle density by electrodeposition time as determined by SEM. (c) Particle size distribution of G/PPy 60, 120, and 360. Particles were grouped into intervals with widths of 10 nm.

20 and 40 nm appearing in addition to the small newly nucleated nanoparticles. The remaining peak at small particle diameters illustrates the continued formation of new nanoparticles as well as the existence of PPy particles that have stabilized between deposition pulses and do not continue growing with subsequent pulses. After 360 s of deposition, a very broad peak forms for particles with a diameter between 10 and 60 nm, further showing that particles are both being enlarged and forming with longer depositions, contributing to the prevalence of relatively small particles. This extended deposition time has the largest frequency of particles with a >40 nm diameter, indicating that particles continue to grow over many deposition pulses. Most notably, very few nanoparticles after this time have diameters under 20 nm, suggesting that nucleation of new nanoparticles is not a major pathway at this point. The high average particle diameter after this deposition time suggests lower redox-active surface area, which will be shown later.

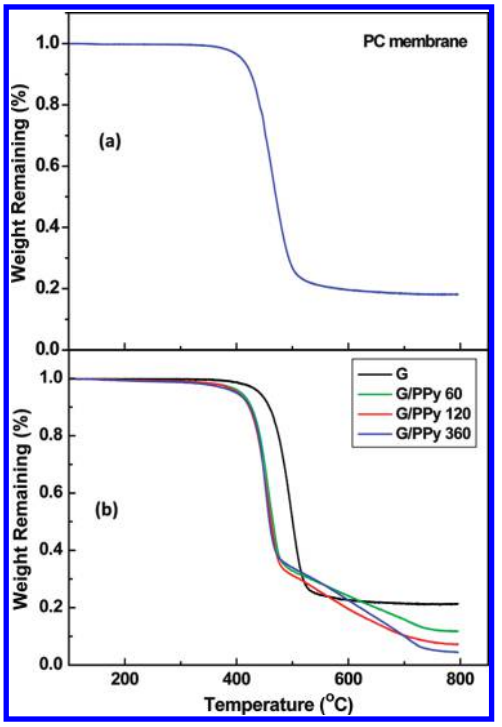

Figure 5. TGA thermograms of (a) PC membrane and (b) G and G/PPy 60, 120, and 360.

TGA was conducted on the samples to verify an increase in the mass of PPy with longer electrodeposition times. The results of TGA in Figure 5a are obtained for a bare PC membrane as a background, whereas Figure 5b yields the results from G and G/PPy 60, 120, and 360, all of which remain adhered to a PC membrane following preparation. Although the weight percentage drops of PC and PPy slightly overlap each other, it remains discernible that the mass of PPy increases in the samples. Indication that the G content makes up a lower percentage of the total mass results from the rate of decreasing mass percent remaining at longer deposition times. As the dimensions of the samples and ratio of G to PC are held constant, the reducing mass that remains after 800 °C is attributed to the increasing deposition mass of PPy in the samples. The presence of PPy may also be seen by the mass loss between 200 and 400 °C and a more notable loss between 550 to 725 °C, which is not present in either the PC or G thermograms.[40] The shift in the mass loss seen in the G thermogram indicates that G has a stabilizing effect on the PC. Within the second weight loss region, a larger slope of the thermograms for longer deposition times is also indicative of an increasing amount of PPy in the sample. The very sharp loss of mass between 450 and 550 °C is attributed to the PC backing membrane, with no degradation prior to or following this temperature range.[48]

Figure 6a−d shows CV curves for pure G and G/PPy 60, 120, and 360 at varied scan rates between −0.4 and 0.6 V versus SCE in 1 M KCl. The CV curve for G is virtually rectangular to show that an approach to ideal and reversible capacitive behavior is achieved.[19] With pulse-deposited PPy, the shapes of CV show double-layer behavior and features of pseudocapacitive activity from PPy between −0.25 and 0.25 V.[17] With extended electrodeposition time, the curve demonstrates a more significant contribution from pseudocapacitive activity of PPy, which is

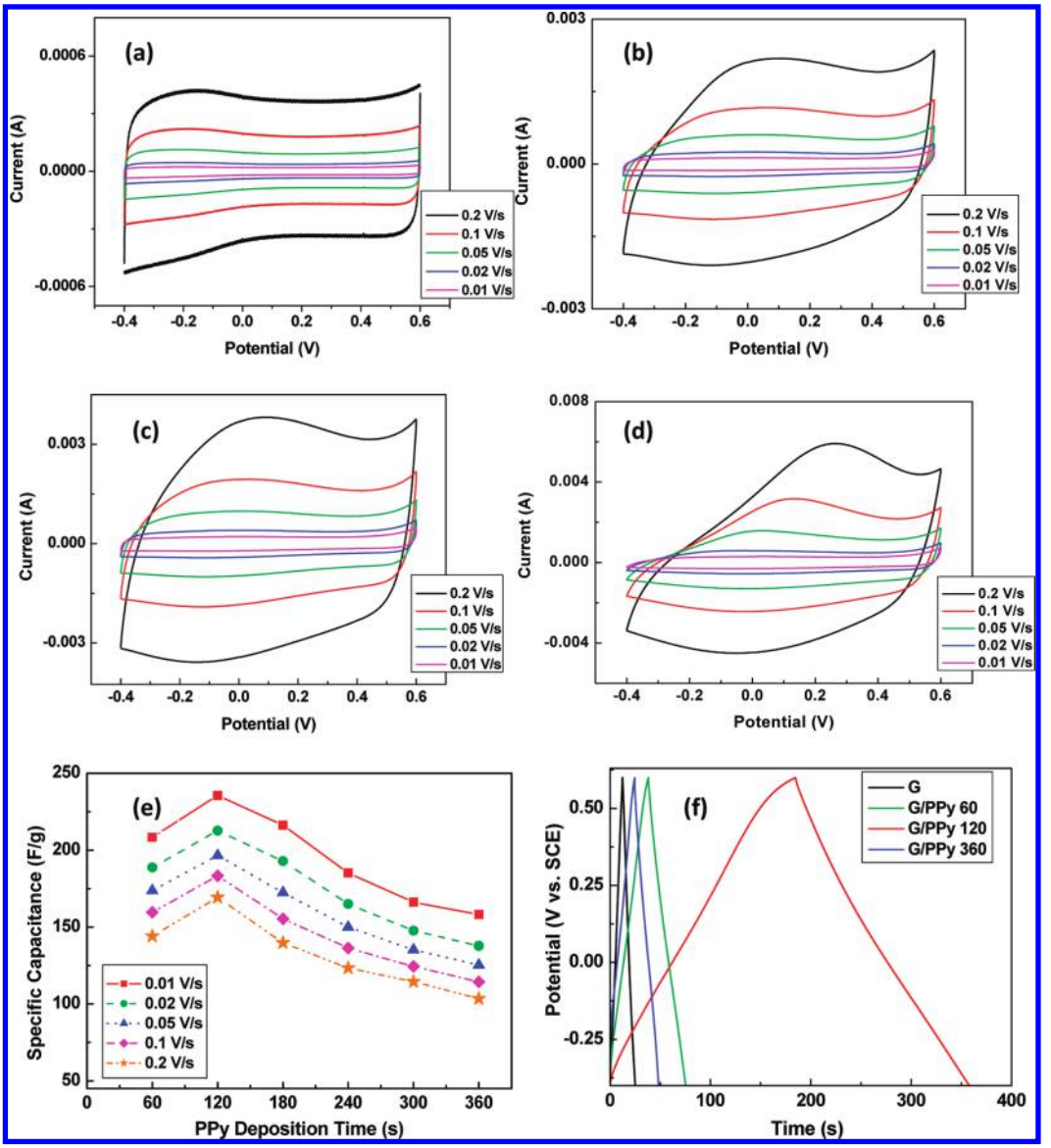

Figure 6. Cyclic voltammogram curves for the (a) G, (b) G/PPy 60, (c) G/PPy 120, and (d) G/PPy 360 electrodes in a KCl solution between −0.4 and 0.6 V versus SCE at scan rates of 0.01, 0.02, 0.05, 0.1, and 0.2 V/s. (e) Specific capacitance of all G/PPy electrodes by electrodeposition time, as determined by CV with different scan rates. (f) Galvanostatic charge−discharge curves for the G, G/PPy 60, G/PPy 120, and G/PPy 360 electrodes for comparison at a current density of 1A/g between −0.4 and 0.6 V versus SCE in 1 M KCl.

consistent with the particle density results shown in Figure 4b. The specific capacitances of the electrodes were determined by CV using the following eq 1[41]

$$C_S = \frac{\int i\,dV}{2*m*\Delta V*S} \quad (1)$$

where C is the specific capacitance in farads per gram, $\int i\,dV$ is the integrated area of the CV curve, m is the mass of the electrode material in grams, ΔV is the scanned potential window in volts, and S is the scan rate in volts per second. Applying this equation to the CV curves for all of the electrodes yields specific capacitances ranging from ~237 F/g for the G/PPy 120 s electrode to ~63 F/g for the graphene electrode at a scan rate of 0.01 V/s. This result demonstrates that with only 120 s of pulse deposition time, the capacity of the graphene film increased almost four times, which is very efficient and cost-effective. The specific capacitance of graphene is slightly lower than what we previously reported for the ultrathin graphene films,[19] probably because of different thickness of the films. Figure 6e shows the specific capacitance values of all of the electrodes at the various scan rates. G/PPy 120 shows the best performance at all scan rates because of the PPy morphology obtained after 120 s of pulsed electrodeposition. As shown by SEM and elaborated on above, G/PPy 120 has a high particle density while still maintaining a relatively low average particle size, leading to a large redox-active surface area able to contribute to the material's pseudocapacitance. The large and densely packed PPy particle growth of G/PPy 360 (Figure 3d) is undesirable for fast ion kinetics and is attributed to the decreased performance.

CD curves in Figure 6f were obtained at a current density of 1 A/g between −0.4 and 0.6 V versus SCE in 1 M KCl for pure G

dx.doi.org/10.1021/jp205568v |J. Phys. Chem. C 2011, 115, 17612–17620

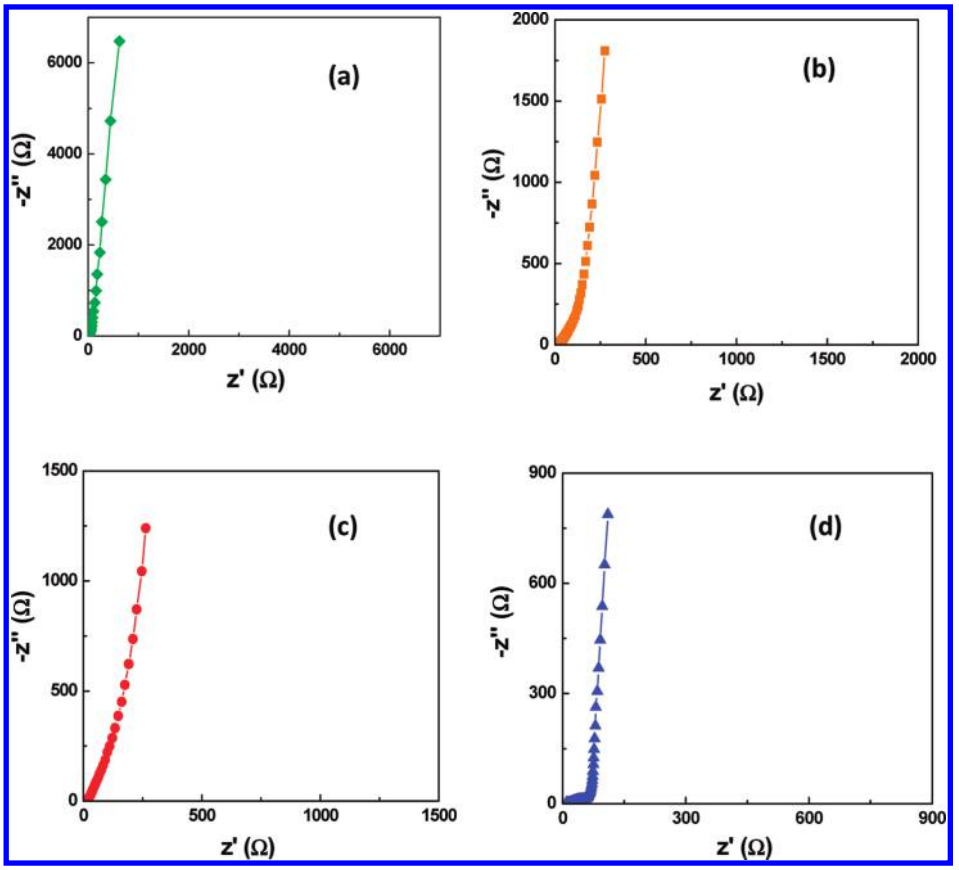

Figure 7. Nyquist plots of the G/PPy electrodes for (a) G, (b) G/PPy 60, (c) G/PPy 120, and (d) G/PPy 360 at frequencies between 1 MHz and 10 mHz with a sinusoidal signal amplitude of 0.01 V versus SCE in 1 M KCl.

and G/PPy 60, 120, and 360. Near-ideal EDLC behavior of the CD curves is seen by the highly linear charge and discharge slopes, where linearity indicates that the rate of change in potential is independent of an applied current.[19] Approach to ideality is also noted by the symmetry of the charge and discharge slopes.[1] The slight curvatures of the slopes of the G/PPy electrodes are indicative of the pseudocapacitive effects of the PPy, and, as expected, the curvatures becomes more pronounced with longer electrodeposition times, indicating increased contribution of pseudocapacitance to the systems. The G/PPy 120 shows a minimal internal resistance (IR) drop upon initiated charge and discharge, illustrating the low contact resistance of the G/PPy composites and efficient use of a capacitance current.[29] This quality reduces the amount of energy lost to contact resistance with each charge/discharge cycle in the form of heat.

Figure 7a−d shows Nyquist plots of the EIS data obtained for pure G and composites G/PPy 60, 120, and 360 at OCP, with a signal amplitude of 10 mV versus SCE within a frequency range of 1 MHz to 10 mHz in 1 M KCl. At low frequencies, the real portion of the impedance approaches a finite value, whereas the imaginary portion of the capacitive reactance impedance nears infinity. This is generally described by an approach of the phase shift angle of impedance to 90°, representing ideal capacitor charging.[14] All EIS plots in Figure 7 are shown to exhibit this behavior at low frequencies, denoting their approach to ideal capacitance. A change of the midrange frequency impedances in both G/PPy 60 and G/PPy 120 gives rise to a visible knee frequency, characteristic of the transition from frequency-dependent diffusion resistance to pure capacitive charging behavior. A Warburg element is often used to describe ion-diffusion resistances and is made apparent by a 45° phase angle. The frequency-dependent diffusion resistance increases with an increase in deposition time as both the number of particles and particle size of PPy continue to increase. The absence of ion diffusion and charge transfer resistances of the untreated graphene sheets contrasts. With a deposition time $t > 300$ s, the electrodeposition of Py is shown to favor increasing the size of existing particles, and the EIS of Figure 7d (G/PPy 360) observes a corresponding increase in the parallel resistances present within the composite. Contributing factors to this resistance include charge transfer resistances and parallel faradaic resistances owing to pseudocapacitive materials. Increasing the size and amount of PPy particles can be expected to increase the diffusion resistance of Cl^- doping ion as well as the related charge-transfer resistance of the redox reaction. It is interesting to note the EIS of shorter deposition times lacks the latter resistance and primarily contributes toward increasing the diffusion resistances, which are attributed to a change in the pore size and structure of individual graphene sheets.

The energy densities of the electrodes were calculated using the following eq 2[6]

$$E = \frac{C \times \Delta V}{7.2} \tag{2}$$

where C is the specific capacitance in farads per gram, ΔV is the potential window in volts, and E is the energy of the electrode in watt hours per kilogram. A high energy density of 32.9 W·h/kg

was derived from CV data for G/PPy 120 and 8.75 W·h/kg for G at a scan rate of 0.01 V/s.

The power densities of the electrodes were calculated from the ratio of energy densities to discharge time as[50]

$$P = \frac{E}{t} \quad (3)$$

where E is the energy density of the electrode in watt hours per kilogram and t is the discharge time of the CV curve in hours, and a power density of 315 and 1184 W/kg were obtained for G and G/PPy 120, respectively, at 0.01 V/s.

CONCLUSIONS

In conclusion, we have presented a simple method to create flexible, uniform G/PPy composite films using a pulsed electrodeposition technique. Specific capacitances as high as 237 F/g were obtained for a moderate deposition time of 120 s. This result compares favorably to studies with much longer and complex processes for deposition of PPy to different carbon scaffolds. G/PPy 120 also exhibited the highest energy with maximum values of ~32.9 W·h/kg, which was notably higher than the values obtained for all other electrodes and compares very favorably to literature values.[14,41] It was clearly shown by SEM that increased electrodeposition time results in increased particle density up to 120 s total deposition time. This increase was attributed to the favorable nucleation of new polymer chains at defects in the graphene surface, which becomes less favorable as defect sites are covered by existing polymer nanoparticles.

With the addition of a pseudocapacitive contribution to graphene supercapacitor electrodes due to a conformal nanoparticle coating of redox-active PPy, it is possible to obtain high power and energy densities while still maintaining the inherent flexibility of graphene films. It is expected that the increases in energy and power densities in a flexible material will lead to numerous applications, especially in the field of personal electronics and renewable energy storage.

ASSOCIATED CONTENT

Supporting Information. Full description of the material. This material is available free of charge via the Internet at http://pubs.acs.org.

AUTHOR INFORMATION

Corresponding Author
*E-mail: aipingyu@uwaterloo.ca.

ACKNOWLEDGMENT

This research was financially supported by the Natural Sciences and Engineering Research Council of Canada (NSERC) and the University of Waterloo.

REFERENCES

(1) Reddy, A. L. M.; Ramaprabhu, S. *J. Phys. Chem. C* **2007**, *111* 7727–7734.
(2) Sharma, R. K.; Rastogi, A. C.; Desu, S. B. *Electrochem. Commun.* **2008**, *10*, 268–272.
(3) Shi, C.; Zhitomirsky, I. *Nanoscale Res. Lett.* **2010**, *5*, 518–523.
(4) Sivakkumar, S. R.; Ko, J. M.; Kim, D. Y.; Kim, B. C.; Wallace, G. G. *Electrochim. Acta* **2007**, *52*, 7377–7385.
(5) Subramanian, V.; Zhu, H. W.; Wei, B. Q. *Electrochem. Commun.* **2006**, *8*, 827–832.
(6) Zhang, L. L.; Zhao, X. S. *Chem. Soc. Rev.* **2009**, *38*, 2520–2531.
(7) Dubal, D. P.; Dhawale, D. S.; Salunkhe, R. R.; Lokhande, C. D. *J. Alloy. Compd.* **2010**, *496*, 370–375.
(8) Frackowiak, E. *Phys. Chem. Chem. Phys.* **2007**, *9*, 1774–1785.
(9) Hu, C. C.; Tsou, T. W. *J. Power Sources* **2003**, *115*, 179–186.
(10) Lee, C. Y.; Tsai, H. M.; Chuang, H. J.; Li, S. Y.; Lin, P.; Tseng, T. Y. *J. Electrochem. Soc.* **2005**, *152*, A716–A720.
(11) Li, G. R.; Feng, Z. P.; Zhong, J. H.; Wang, Z. L.; Tong, Y. X. *Macromolecules* **2010**, *43*, 2178–2183.
(12) Masarapu, C.; Zeng, H. F.; Hung, K. H.; Wei, B. Q. *Acs Nano* **2009**, *3*, 2199–2206.
(13) Roberts, A. J.; Slade, R. C. T. *J. Mater. Chem.* **2010**, *20*, 3221–3226.
(14) Wang, Y.; Shi, Z.; Huang, Y.; Ma, Y.; Wang, C.; Chen, M.; Chen, Y. *J. Phys. Chem. C* **2009**, *113*, 13103–13107.
(15) Du, Q. L.; Zheng, M. B.; Zhang, L. F.; Wang, Y. W.; Chen, J. H.; Xue, L. P.; Dai, W. J.; Ji, G. B.; Cao, J. M. *Electrochim. Acta* **2010**, *55*, 3897–3903.
(16) Jiang, J. H.; Kucernak, A. *Electrochim. Acta* **2002**, *47*, 2381–2386.
(17) Kim, J. H.; Nam, K. W.; Ma, S. B.; Kim, K. B. *Carbon* **2006**, *44*, 1963–1968.
(18) Kaempgen, M.; Chan, C. K.; Ma, J.; Cui, Y.; Gruner, G. *Nano Lett.* **2009**, *9*, 1872–1876.
(19) Yu, A. P.; Roes, I.; Davies, A.; Chen, Z. W. *Appl. Phys. Lett.* **2010**, *96*, 253105–253108.
(20) Raymundo-Pinero, E.; Khomenko, V.; Frackowiak, E.; Beguin, F. *J. Electrochem. Soc.* **2005**, *152*, A229–A235.
(21) Dubal, D. P.; Dhawale, D. S.; Salunkhe, R. R.; Pawar, S. M.; Lokhande, C. D. *Appl. Surf. Sci.* **2010**, *256*, 4411–4416.
(22) Huang, J. S.; Sumpter, B. G.; Meunier, V. *Angew. Chem., Int. Ed.* **2008**, *47*, 520–524.
(23) Konno, H.; Ito, T.; M., U.; K., F.; K., A. *J. Power Sources* **2010**, *195*, 1739–1746.
(24) Li, F. H.; Song, J. F.; Yang, H. F.; Gan, S. Y.; Zhang, Q. X.; Han, D. X.; Ivaska, A.; Niu, L. *Nanotechnology* **2009**, *20*, 455602.
(25) Zhang, Y. P.; Li, H. B.; Pan, L. K.; Lu, T.; Sun, Z. *J. Electroanal. Chem.* **2009**, *634*, 68–71.
(26) Li, D.; Muller, M. B.; Gilje, S.; Kaner, R. B.; Wallace, G. G. *Nat. Nanotechnol.* **2008**, *3*, 101–105.
(27) Shen, J. F.; Hu, Y. H.; Li, C.; Qin, C.; Ye, M. X. *Small* **2009**, *5*, 82–85.
(28) Si, Y.; Samulski, E. T. *Nano Lett.* **2008**, *8*, 1679–1682.
(29) Wu, Q.; Xu, Y. X.; Yao, Z. Y.; Liu, A. R.; Shi, G. Q. *ACS Nano* **2010**, *4*, 1963–1970.
(30) Ansari, S.; Giannelis, E. P. *J. Polym. Sci., Polym. Phys.* **2009**, *47*, 888–897.
(31) Park, S.; An, J. H.; Jung, I. W.; Piner, R. D.; An, S. J.; Li, X. S.; Velamakanni, A.; Ruoff, R. S. *Nano Lett.* **2009**, *9*, 1593–1597.
(32) Schniepp, H. C.; Li, J. L.; McAllister, M. J.; Sai, H.; Herrera-Alonso, M.; Adamson, D. H.; Prud'homme, R. K.; Car, R.; Saville, D. A.; Aksay, I. A. *J. Phys. Chem. B* **2006**, *110*, 8535–8539.
(33) Stankovich, S.; Piner, R. D.; Chen, X. Q.; Wu, N. Q.; Nguyen, S. T.; Ruoff, R. S. *J. Mater. Chem.* **2006**, *16*, 155–158.
(34) Tung, V. C.; Allen, M. J.; Yang, Y.; Kaner, R. B. *Nat. Nanotechnol.* **2009**, *4*, 25–29.
(35) Stankovich, S.; Dikin, D. A.; Dommett, G. H. B.; Kohlhaas, K. M.; Zimney, E. J.; Stach, E. A.; Piner, R. D.; Nguyen, S. T.; Ruoff, R. S. *Nature* **2006**, *442*, 282–286.
(36) Nam, K. W.; Lee, C. W.; Yang, X. Q.; Cho, B. W.; Yoon, W. S.; Kim, K. B. *J. Power Sources* **2009**, *188*, 323–331.
(37) Qu, Q. T.; Zhang, P.; Wang, B.; Chen, Y. H.; Tian, S.; Wu, Y. P.; Holze, R. *J. Phys. Chem. C* **2009**, *113*, 14020–14027.
(38) Zhang, J.; Kong, L.-B.; Li, H.; Luo, Y.-C.; Kang, L. *J. Mater. Sci.* **2010**, *45*, 1947–1954.
(39) Han, Y. Q.; Qing, X. T.; Ye, S. J.; Lu, Y. *Synth. Met.* **2010**, *160*, 1159–1166.

(40) Mavinakuli, P.; Wei, S. Y.; Wang, Q.; Karki, A. B.; Dhage, S.; Wang, Z.; Young, D. P.; Guo, Z. H. *J. Phys. Chem. C* **2010**, *114*, 3874–3882.
(41) Yan, J.; Wei, T.; Fan, Z.; Qian, W.; Zhang, M.; Shen, X.; Wei, F. *J. Power Sources* **2010**, *195*, 3041–3045.
(42) Fang, Y. P.; Liu, J. W.; Yu, D. J.; Wicksted, J. P.; Kalkan, K.; Topal, C. O.; Flanders, B. N.; Wu, J. D.; Li, J. *J. Power Sources* **2010**, *195*, 674–679.
(43) Hummers, W. S.; Offeman, R. E. *J. Am. Chem. Soc.* **1958**, *80*, 1339–1339.
(44) Wang, D. W.; Li, F.; Lui, M.; Cheng, H. M. *New Carbon Mater.* **2007**, *22*, 307–314.
(45) Cui, L. L.; Lu, X. F.; Chao, D. M.; Liu, H. T.; Li, Y. X.; Wang, C. *Phys. Status Solidi A* **2011**, *208*, 459–461.
(46) Massa, M. V.; Carvalho, J. L.; Dalnoki-Veress, K. *Phys. Rev. Lett.* **2006**, 97.
(47) Gouldstone, A.; Vliet, K. J. V.; Suresh, S. *Nature* **2001**, *411*, 656.
(48) Jang, B. N.; Wilkie, C. A. *Polym. Degrad. Stab.* **2004**, *86*, 419–430.
(49) Zhou, H. H.; Chen, H.; Luo, S. L.; Lu, G. W.; Wei, W. Z.; Kuang, Y. F. *J. Solid State Electrochem.* **2005**, *9*, 574–580.
(50) Yan, J.; Fan, Z. J.; Wei, T.; Cheng, J.; Shao, B.; Wang, K.; Song, L. P.; Zhang, M. L. *J. Power Sources* **2009**, *194*, 1202–1207.